Computational aeroacoustics: The low speed jet

E. J. Avital
School of Engineering and Materials
University of London
London, UK

M. Alonso
Mott McDonald
Croydon, UK

V. Supontisky
School of Engineering Sciences
University of Southampton,
Southampton, UK

ABSTRACT

Low speed circular, elliptic and planar jets are investigated computationally for basic sound generation and hydrodynamics. The jets are assumed to be incompressible and are simulated using the large eddy simulation (LES) approach. The emitted sound is calculated using Lighthill's acoustic analogy. Two formulations are used, Lighthill's stress tensor formulation and Powell's vortex sound formulation. A new boundary correction for Powell's formulation is developed in order to account for the finite size of the computational domain. Low to moderate Reynolds number jets are simulated. Good agreement with known hydrodynamic results is achieved. This includes the nature of the transition process, e.g. enhanced mixing and axis switching in the elliptic jet and in some statistical results. The new boundary correction for Powell's formulation proves to be vital in order to achieve good agreement with Lighthill's formulation. Some success in high frequency prediction at least for the circular and elliptic jets is achieved in terms of getting the expected asymptotic behaviour. Both formulations show that the elliptic jet noise level is mildly lower than the circular jet noise level. Good to very good agreement is achieved in terms of directivities and frequency spectra with known results for the various jets.

NOMENCLATURE

b	planar jet's local half width
c_0	ambient speed of sound
C_1	slope coefficient in the asymptotic linear distribution of the planar jet's centreline velocity.
C_2	constant in the asymptotic linear distribution of the planar jet's centreline velocity.
D	jet's diameter
$D(\theta)$	directivity
f	frequency
f_j	forcing term in Powell's boundary correction
h	width of the planar jet's nozzle
I	mean acoustic intensity
K_1	slope coefficient in the asymptotic linear distribution of the planar jet's half width
K_2	constant in the asymptotic linear distribution of the planar jet's half width
P	acoustic power output
Q_{ij}	quadrupole source
R	effective radius of the jet's inflow profile
Re	Reynolds number

Paper No. 3260. Manuscript received 16 November 2007, revised 17 February 2008 accepted 20 March 2008.
A version of this paper was presented as an invited lecture at the two-day conference
to celebrate 100 years of Aeronautics at Queen Mary College on 10-11 September 2007.

https://doi.org/10.1017/S0001924000002360 Published online by Cambridge University Press

S	surface area
St	Strouhal number
T	normalised time unit in the LES simulation
T_{ij}	Lighthill's stress tensor
T	time
U_0	Jet's mean centreline velocity at the inflow
$\overline{U}_{c.l.}$	Jet's mean centreline velocity
x	location in the sound field
$\overline{x}$	streamwise direction in the computational LES domain
y	location of the sound source
y	streamnormal direction in the computational LES domain
z	spanwise direction in the computational LES domain
θ	polar angle
ρ	density
ρ_0	ambient density
ρ'	sound density fluctuations
ϕ	spherical angle
ω	vorticity

1.0 INTRODUCTION

Aeroacoustics deals with sound generated by fluid flow such as jets, wakes and boundary layers. The introduction of the jet engine in the late 40s led to a significant increase in aeroacoustics research. One of the early mathematical formulations is Lighthill's acoustic analogy[1]. It is widely used nowadays and it relates the sound source to the fluctuations in the velocity stress tensor. A few years later Lilley[2] published a report on subsonic jet noise looking for similarity laws and source distribution using that formulation. Powell[3] introduced a vortex sound formulation in conjunction with Lighthill's acoustic analogy. It related the source to the fluctuations of the cross product between the vorticity field and sound field. This was further developed by Möhring for cold low speed flows showing how the source can be expressed only by the vorticity field[4]. An important development in the early 70s was Lilley's equation[5] which took explicitly into account convection and shear refraction effects unlike Lighthill's equation. The fast development of computational power in the early 90s led to a new field of computational aeroacoustics (CAA) which Lighthill defined as the start of a second golden age in aeroacoustics[6]. For a recent review on CAA the author is referred to a comprehensive review by Wang *et al*[7]. In this paper we will look at CAA of low speed jets as carried out in Queen Mary, University of London.

Crighton[8] pointed out the importance of CAA of low speed jet noise by arguing that higher subsonic speed effects can be added through Doppler correction terms and shear refraction correction. The challenge is to calculate and investigate the underlying physics of the sound generation. Low speed flow noise exhibits unique computational challenges because of the very large difference between the source (flow) field and the sound field in energy level and length scale. The emitted sound energy is much lower than the hydrodynamic energy level and the emitted sound wave length is much larger than the flow length scale. Therefore an indirect or a split approach is appropriate where the flow field is calculated using a computational fluid dynamics (CFD) method and the emitted sound is calculated using an aeroacoustic method. In this study the large eddy simulation (LES) method is used to simulate the flow. In LES the large scale flow structures are resolved and the small scale structures are modelled. Lighthill's acoustic analogy is then used to calculate the emitted sound from the flow large scale structures, where computational issues such as the finite size of the computational domain have to be accounted for. This approach can be used for other types of shear flows such as cavity flow e.g. Supontisky *et al*[9] or Lai and Luo[10]. The first study used the Lighthill-Curle's formulation and the second study used the more general Ffowcs Williams/Hawkings equation. Both formulations can be seen as extensions to the Lighthill's formulation to account for the effects of wall boundaries.

Circular, elliptic and planar jets will be investigated. Circular jets are very common in aeronautical applications and subsonic jet noise has been considerably investigated. Crow and Champagne[11Z] were among the firsts to identify the occurrence of large scale structures in turbulent jets. This finding challenged the view that the sound source in free shear flow is composed of small uncorrelated eddies. Kibens[12] studied experimentally the role of the large structures, showing that by exciting the jet, distinctive peaks appear in the frequency spectrum of the far sound field. Laufer and Yen[13] identified large scale structures as being responsible for a considerable part of the low frequency noise emission. Their data was further analysed by Crighton and Huerre[14] to yield a simple two dimensional wave packet model, establishing the notation of a superdirective sound field. This was further investigated analytically by Avital and Sandham[15] to identify the dependence of the penetration length of the near sound field on the wave packet form. A computational indirect approach was used by Avital *et al*[16] to investigate the sound emitted by axisymmetric low speed jets of low Reynolds number. It was shown that the finite size of the computational domain has to be considered when implementing Lighthill's analogy. A boundary correction was developed for Möhring's formulation and the axisymmetric case. Jiang *et al*[17] also used an indirect approach where the acoustic method was based on simulating in time Lilley's equation. They achieved good agreement between the prediction of Lilley's equation and results from compressible Direct Numerical Simulation (DNS) for subsonic axisymmetric jets.

Elliptic jets of aspect ratio 2:1 with a Reynolds number $Re_D = 7\times8\cdot10^4$ were studied experimentally by Ho and Gutmark[18], observing enhanced mixing and axis-switching. Axis-switching occurred three times in the region $0 < x/a < 40$, where 2a is the major axis of the jet. A comparison between elliptic and equivalent circular jets showed a mass entrainment several times higher in the elliptic jet. Bridges and Hussain[19] investigated experimentally vortex pairings in elliptic jets, finding that the emitted sound was almost axisymmetric. Tam and Zaman[20] investigated analytically and experimentally subsonic asymmetric jet configurations. They concluded that modifying the nozzle geometry to an elliptic or a rectangular profile is less effective in reducing jet noise than tabbed nozzles.

Probably the most comprehensive experimental study on the transition of a planar jet was conducted by Sato[21]. The effect of the shape of the velocity profile at the nozzle's exit was found to be important in determining whether the transition goes through a symmetric or an antisymmetric mode. The occurrence of large scale structures in the self preserving region of the planar jet was also identified[22]. A corresponding correlation frequency was observed to stay almost constant when it was scaled by the centreline mean velocity and the local width of the jet. Only limited hydrodynamic computational studies were carried out, e.g. the DNS study of Stanley *et al*[23]. On the aeroacoustics side, Kouts and Ku[24] and Munro and Ahuja[25] investigated experimentally very high aspect ratio rectangular jets, providing two dimensional directivities and frequency spectra for the emitted sound.

The aims of the current study are to assess the capability of implementing Lighthill's and Powell's formulations along with LES simulation and to investigate the generation of basic sound pattern, i.e. without convection and shear refraction effects. The effect of changing the inflow profile from circular to elliptic will be investigated as well as looking at the case of a high aspect ratio rectangular jet, modelled as a planar jet.

2.0 NUMERICAL FORMULATION

2.1 Hydrodynamic formulation

Because of the low speed assumption the Navier Stokes (NS) equations were taken as incompressible as in Avital *et al*[16]. In

https://doi.org/10.1017/S0001924000002360 Published online by Cambridge University Press

essence the flow field is then separated from the sound field requiring us to use an auxiliary aeroacoustic method such as the acoustic analogy to calculate the sound field. This approach is based on the Möhring's approach taking that the fluctuations in the vorticity field are the major source in generating the basic far field sound pattern. Thus similar to the derivation of Möhring's formulation[4], the velocity flow field is taken as divergence free.

Our in-house code Lithium in its structured finite difference staggered grid form was used. The spatially filtered NS equations were marched in time using a compact third order Runge Kutta method[26]. The projection method was used to ensure continuity. In order to solve the pressure equation, a solver based on the fast fourier transform (FFT) was used, capable of dealing with a non uniform grid and embedded rigid bodies[27]. The convection and diffusion terms were calculated using 4th order differences and central schemes respectively similar to those used in the LES study of Kim and Menon[28]. The mixed time scale (MTS) sub grid scale model of Inagkai *et al*[29] was used to model the effect of the small structures on the resolved large scale structures. In addition a passive scalar was simulated in order to provide illustration for the flow development.

Zero pressure boundary conditions were used at the stream normal direction and for the circular and elliptic jets in the spanwise direction too. Periodic spanwise boundary conditions were used for the planar jet. A simple 1D outflow boundary condition was used at the outlet of the computational domain. In order to minimise its effect a buffer zone was added in front of the outlet, taking about 15% of the computational domain, see for example Fig. 1. In the buffer zone the calculation of the convection terms was switched gradually in the x direction from a 4th order scheme at the start of the buffer zone to a first order upwind scheme at the end of the buffer zone which was also the outlet of the computational domain. The xx diffusion term was gradually damped to zero in a similar way. The source term in the pressure equation was also damped similarly to zero in order to prevent reflections into the domain of the physical meaning. If a rigid body was introduced into the computational domain as in the case of the planar jet, its boundaries coincided with the grid lines. No slip velocity boundary conditions with a second order accuracy were implemented by specifying fictitious values for the velocity field inside the rigid body. Further details on the hydrodynamic formulation are in Avital[27] and Supontisky *et al*[30].

2.2 Aeroacoustic formulation

Following Lighthill's formulation for cold low speed flow and assuming a compact source one can write;

$$\rho'(\bar{x},t)=\frac{x_i x_j}{4\pi|\bar{x}|^3 c_0^4}\left[\int\frac{\partial^2 T_{ij}\left(\bar{y},t-|\bar{x}|/c_0\right)}{\partial t^2}\mathrm{d}\bar{y}+BC_L\right],\ T_{ij}=\rho_0 u_i u_j \qquad \ldots(1)$$

ρ' is the acoustic density fluctuation at point $\bar{x}$ and c_0 is the ambient speed of sound. The boundary correction BC_L in Equation (1) is needed since the computational domain is finite. According to Lighthill's theory, subsonic eddies generate noise due to modulations in the form and not due to steady convection (unlike in supersonic eddies). Therefore if a boundary correction is not used eddies leaving the domain will simply disappear from the integration which may lead to the calculation of spurious noise. On the other hand, if we neglect the effect of the flow outside the computational domain we can also assume that it does not generate sound. Thus we will use a boundary correction based on assuming a frozen convecting structure leading to[16]:

$$BC_L=\int_{S_{out}}\frac{\partial T_{ij}}{\partial t}U_c\cdot\mathrm{d}s-\int_{S_{in}}\frac{\partial T_{ij}}{\partial t}U_c\cdot\mathrm{d}s \qquad \ldots(2)$$

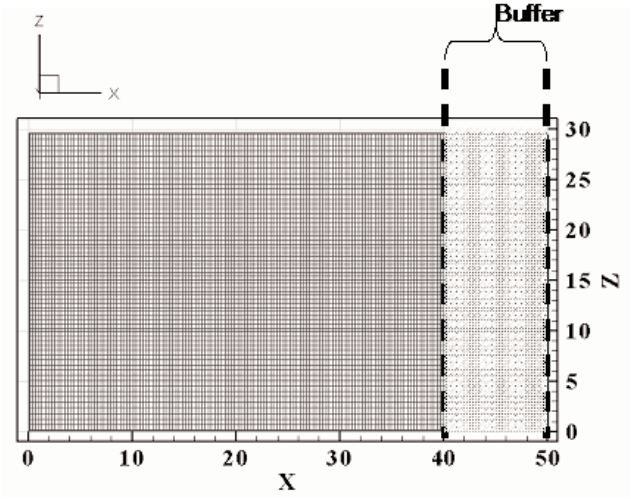


Figure 1. Typical mesh used for the circular and elliptic jets simulation. The computational domain size is of $50R\times 30R\times 30R$ containing $320\times 193\times 193$ points in the x, y and z directions. Note that only $160\times 86\times 86$ grid points are shown for clarity.

S_{out} is the outlet surface area of the computational domain and S_{in} is the inlet. U_c is a mean convective velocity and it usually varies between 0·5 as 0·7 of the centreline velocity. In this study U_c was taken as 0·7 as in Avital *et al*[16]. Changing it to 0·5 or neglecting the inlet integral was found to have a small effect, i.e. much less than 0·5 dB in the frequency spectra and directivity, which is less than the difference between the two aeroacoustic formulations as illustrated in the Results section.

Powell's formulation is analytically identical to Lighthill's and can be expressed as:

$$\rho'(\bar{x},t)=\frac{-\rho_0 x_i x_j}{4\pi|\bar{x}|^3 c_0^4}\left[\frac{\partial^2}{\partial t^2}\int y_i\left(\bar{\omega}\times\bar{u}\right)_i\left(\bar{y},t-\frac{|\bar{x}|}{c_0}\right)\mathrm{d}\bar{y}+BC_p\right] \qquad \ldots(3)$$

As observed by Avital *et al*[16] the vortex sound formulation exhibits dependency on the origin of the coordinates. In an infinite space as assumed by Powell this dependency disappears but for a finite computational domain it may not. The dependency in Equation (3) on y_i is linear and thus can be tackled as Möhring's formulation was dealt with for the axisymmetric case[16]. Since in a jet simulation the computational domain is generally large in the directions normal to streamwise direction, this artificial dependency will occur only in the streamwise direction. The new boundary correction is taken in the form of;

$$BC_p=\int_{S_{out}}(y_1-y_{01})f_j\mathrm{d}s-\int_{S_{in}}(y_1-y_{01})f_j ds \qquad \ldots(4)$$

y_1 is the streamwise co-ordinate and y_{01} is the location of the co-ordinate origin in that direction. Following the derivation in Appendix A one gets:

$$f_1=-\frac{1}{2}\frac{\partial^2\left(u_1^2-u_2^2-u_3^2\right)}{\partial t^2},\ f_2=-\frac{\partial^2\left(u_1u_2\right)}{\partial t^2},\ f_3=-\frac{\partial^2\left(u_1u_3\right)}{\partial t^2} \qquad \ldots(5)$$

Once ρ' is found, the acoustic power output P can be calculated as:

$$P=\int_0^{\pi}D(\theta)\mathrm{Sin}\theta d\theta,\ D(\theta)=\int_0^{2\pi}I|\bar{x}|^2 d\phi,\ I=c_0^3\overline{\rho'^2}/\rho_0 \qquad \ldots(6)$$

θ is the polar angle relative to the streamwise direction and ϕ is the spherical angle. D is the directivity and I is the mean acoustic intensity.

https://doi.org/10.1017/S0001924000002360 Published online by Cambridge University Press

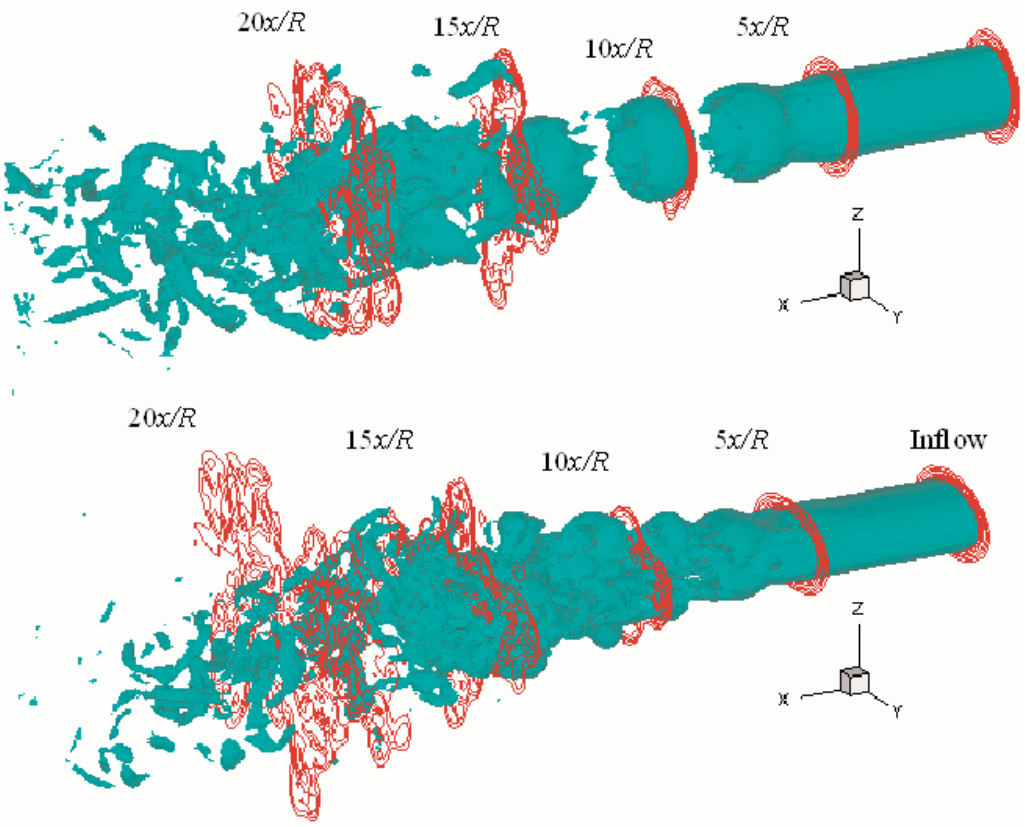


Figure 2. Instantaneous vorticity iso-surface for the circular (above) and elliptic (below) jets at normalised time 340 and Re_D = 6,000. Slices shown, from right to left respectively are at: inflow, 5R*R*, 10*R*, 15*R* and 20*R* (there are 15 levels from maximum to minimum).

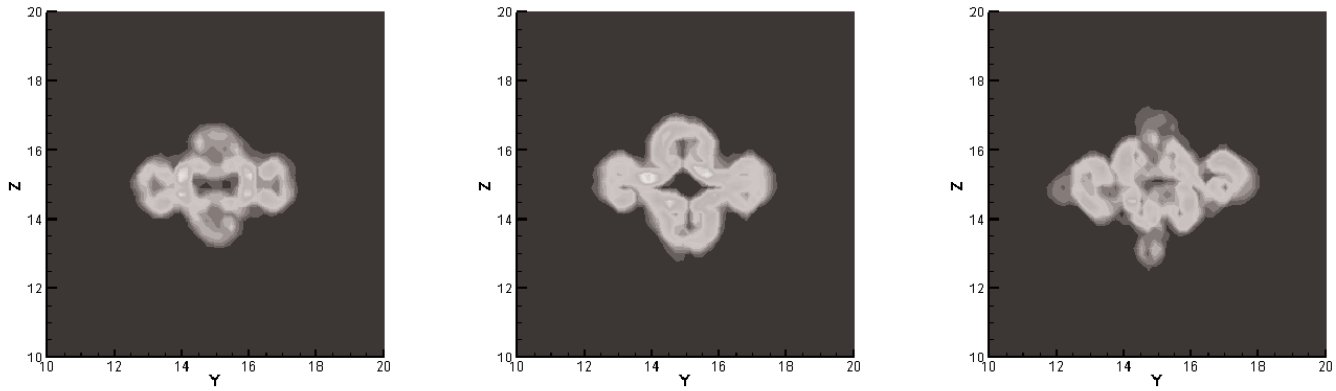


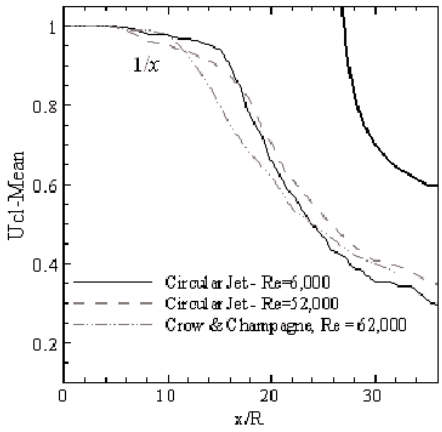
Figure 3. Instantaneous vorticity iso-surface for the circular (above) and elliptic (below) jets at normalised time 340 and Re_D = 6,000. Slices shown, from right to left respectively are at: inflow, 5*R*, 10*R*, 15*R* and 20*R* (there are 15 levels from maximum to minimum).

3.0 RESULTS

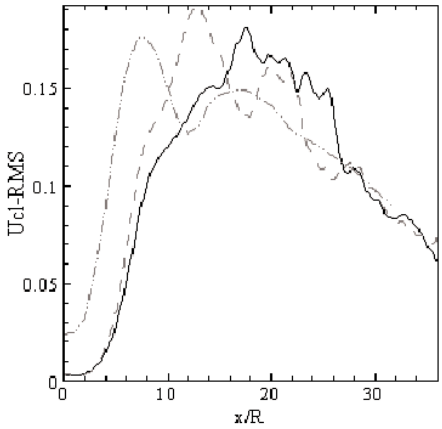
3.1 Free circular and elliptic jets

A computational domain of the size (50*R*, 30*R*, 30*R*) was set in the streamwise, stream normal and spanwise directions respectively as illustrated in Fig. 1. *R* is the effective radius of the inflow profile, where for the elliptic jet it is the radius of the equivalent circle with the same area. Grid sizes of (320, 193, 193) and (480, 193, 193) points were used where grid convergence was checked by comparing results between the two grids and results from different grid mappings. In the following results grid points were clustered near the jet's centreline yielding a 1 to 1·5 ratio between the grid spacing at the center line to the grid spacing at the stream-normal and spanwise boundaries of the computational domain. The jet inflow profile was set to a hyperbolic tangent profile with a momentum thickness of 10% of the local radius[31]. An elliptic profile of aspect ratio of 2:1 was achieved by elongating that profile. The transverse inflow velocities were set to zero. The inflow profile was perturbed using four discrete frequencies spaced between $0{\cdot}175 < St_D < 0{\cdot}425$ and with a combined amplitude peak of 2% relative to the mean velocity, where $St_D = f\,U_0/D$. A phase function randomised in space was introduced into the disturbance in order to enhance the generation of small scale structures and to prevent phase locking between the frequencies. The simulations started from a state of parallel flow and the transient structures were allowed to leave the computational domain before starting the statistics and aeroacoustic calculations. These calculations were carried out for $240 < T < 340$, where one time unit T is equal to R/U_0.

https://doi.org/10.1017/S0001924000002360 Published online by Cambridge University Press



(a)



(b)

Figure 4. Downstream evolution of (a) the mean (b) and the RMS of the centreline velocity of the circular jet. Also shown are (dash double dotted) Crow and Champag\ne's experimental results $Re_D = 62{,}000$.

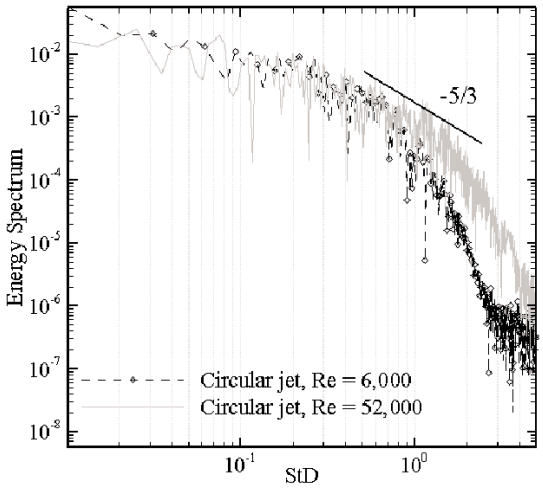
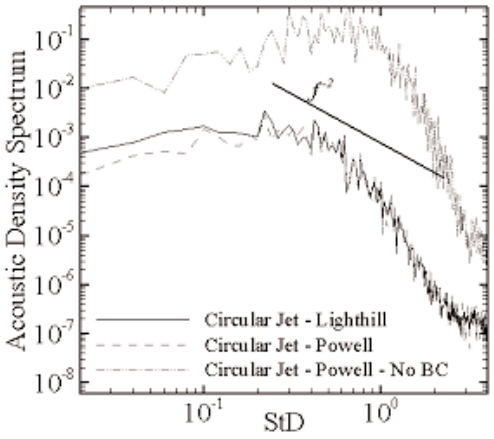
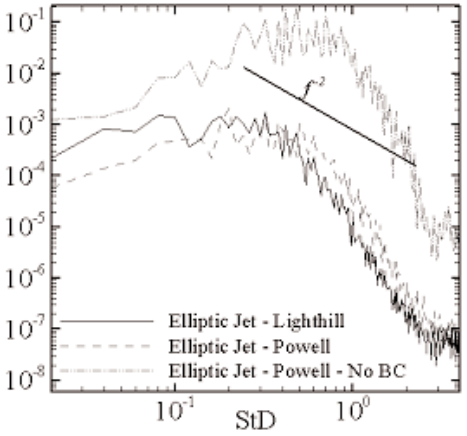


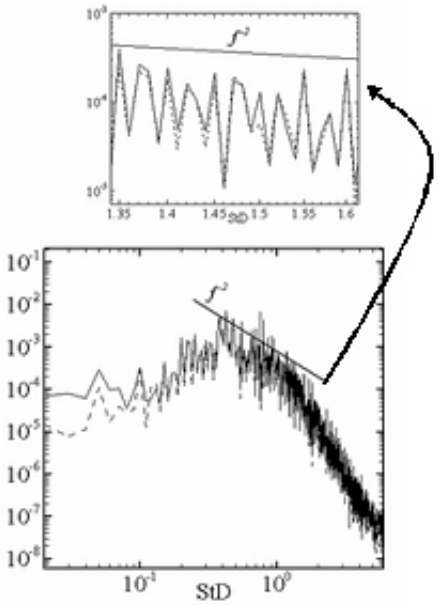
Figure 5. Energy spectrum at a tracking point located on the centreline at a downstream position of 30*R* of the circular jet.



(a)



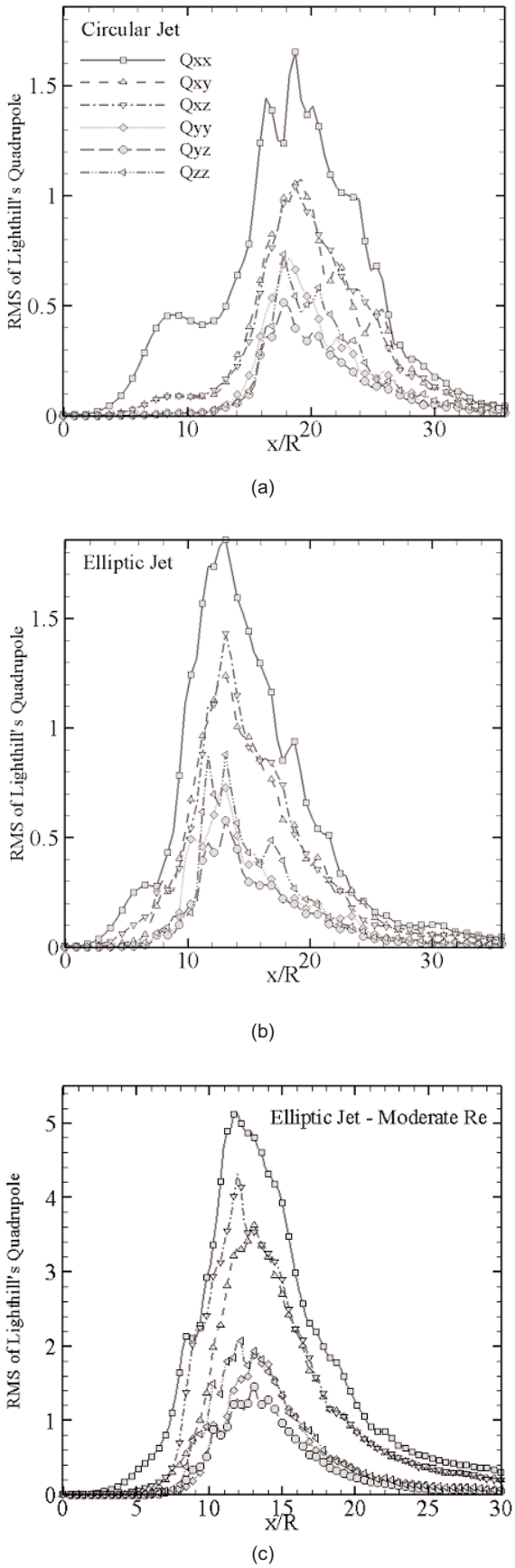
(b)



(c)

Figure 6. Acoustic density frequency spectrum for (a) the circular jet of $Re_D = 6{,}000$, (b) the elliptic jet of $Re_D = 6{,}000$ and (c) the elliptic jet of $Re_D = 52{,}000$. Solid line is the result of Lighthill's formulation and dashed line is of Powell's formulation.

https://doi.org/10.1017/S0001924000002360 Published online by Cambridge University Press



Figures 7. Source location: variation of Lighthill's quadrupoles' RMS in the streamwise direction for (a) the circular jet of Re_D = 6,000, (b) the elliptic jet of Re_D = 6,000 and (c) the elliptic jet of Re_D= 52,000.

Typical instantaneous iso-surfaces are shown in Figs 2. Both circular and elliptic jets show transition to turbulence through a puffing mode mechanism. However the elliptic jet shows earlier transition due to the enhanced mixing that is typical for elliptic jets[18]. A mild axis switching was observed in the elliptic jet around $x = 11R$ as indicated by the elongation of the minor axis seen in the cross-section contours of Fig. 3. Any axis switching after $15R$ is hindered by the jet transition.

The downstream evolution of the centreline velocity is shown for the circular jet in Figs 4. It is seen that both jets of Re_D = 6,000 and 52,000 enter the transition region where the mean centreline velocity decays as $1/x$. Due to the higher mixing in the higher Reynolds number jet, the centreline velocity decays earlier. The agreement with the experimental result of Crow and Champagne[11] is good but not excellent which may be because of different inflow conditions. From the Root Mean Square (RMS) plot of Fig. 4(b) it can be seen that increasing the Reynolds number indeed pushes the RMS peak upstream and generates a double peak structure as it was observed in experiments. The elliptic jet showed a similar behaviour but with a rather unexpected moderate decrease of about 15% in the RMS peak because of the increase in the Reynolds number from 6,000 to 52,000.

The flow energy spectra for the circular jet are shown in Fig. 5. A fair agreement with the Kolmogorov's slope of –5/3 is achieved, although a clearer agreement should be expected in a higher Reynolds number. As expected the jet flow of Re_D = 52,000 shows higher level of energy in the higher frequency range. This points to a higher generation of small scale structures. It comes slightly at the expense of the energy level at lower frequencies. The elliptic jet showed a similar behaviour.

The acoustic density spectra for the overall acoustic power are shown in Figs 6 where the factor involving c_0 was taken out. It is clearly seen that without the new boundary correction for Powell's formulation, the latter can predict much higher levels of acoustic energy than the prediction of Lighthill's formulation. On the other hand, when the new boundary correction is used, very good to excellent agreement is achieved between the two predictions, particularly for the higher frequency range. Both formulations and both circular and elliptic jets manage to achieve the asymptotic slope of f^2 as expected for low Reynolds numbers[32]. Increasing the Reynolds number leads to a noticeable peak around St_D = 0·3 as can be seen for the elliptic jet in Fig. 6(c).

The streamwise distributions of the RMS of Lighthill's quadrupoles Q_{ij} are shown in Figs 7. Q_{ij} are defined as $\partial^2 T_{ij}/\partial t^2$ and the RMS was summed in the stream normal and spanwise directions. Both circular and elliptic jets show a dominance of the streamwise longitudinal quadrupole Q_{xx}. All quadrupoles show a peak around $x = 18R$ for the circular jet and $x = 12R$ for the elliptic jet. Thus they show a peak after the end of the potential core as expected[15]. Increasing the Reynolds number leads to a significant increase in the RMS levels of the quadrupoles as can be seen for the elliptic jet in Fig. 7(c). However it does not cause a significant change in the location of the quadrupoles' peaks.

The resulted directivity patterns $D(\theta)$ are shown in Fig. 8. Both jets and both acoustic formulations show higher emission in the streamwise direction due to the dominance of streamwise longitudinal quadrupole Q_{xx}. The agreement between Lighthill and Powell formulation is very good giving a consistent difference of up to about 1dB in both jets. However there is a disagreement between the profiles near the stream-normal direction ($\theta \cong 90°$). This is because of a difference in the relative strength of the quadrupoles in each formulation. Nevertheless, both formulations show that the circular jet noise level is only about 2dB higher than the elliptic jet in general. Considering that by Fig. 8 the accuracy of the prediction is no less than 1dB, this therefore agrees with Tam and Zaman's conclusion[20] that changing the profile of the nozzle from circular to elliptic may not be very effective for noise reduction as compared to the tabbed nozzle approach. Although one should keep in mind that the results shown in Figs 8 are for a low Reynolds number.

https://doi.org/10.1017/S0001924000002360 Published online by Cambridge University Press

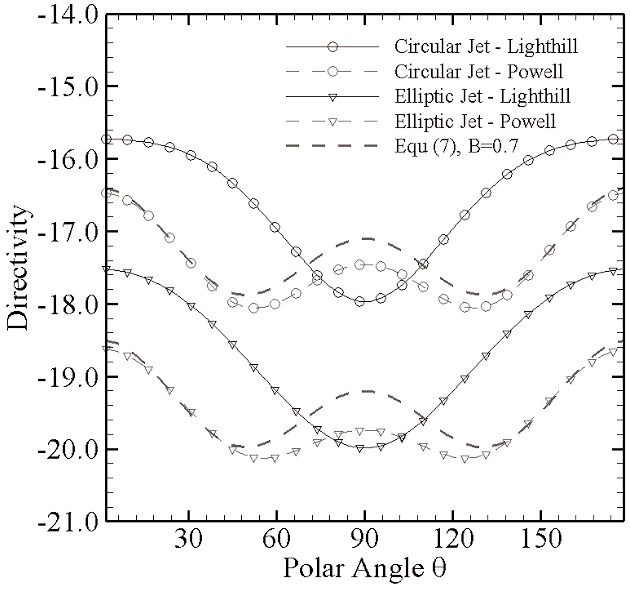


Figure 8. Directivity pattern of sound radiation averaged in the azimuthal direction for the circular and elliptic jets of Re_D= 6,000.

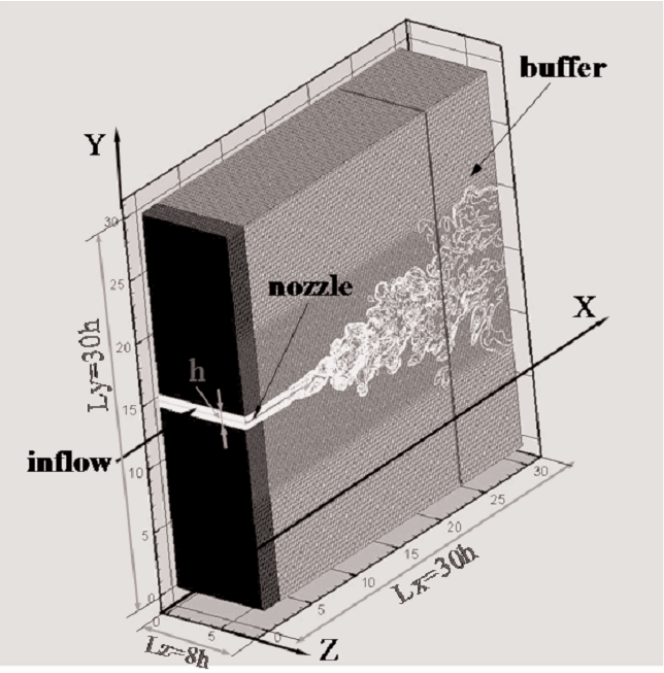


Figure 9. Typical computational domain and grid that were used for the planar jet simulations. Also shown are typical instantaneous contours of the simulated passive scalar, illustrating the jet breakdown to small scales.

Musafir[33] suggested the following relation for a normalised directivity of low speed circular jets;

$$D(\theta) = 1 + B\mathrm{Cos}^4\theta - \frac{B+3}{4}\mathrm{Sin}^2(2\theta) \quad \ldots (7)$$

The value of B = 0·7 was suggested as it fitted experimental results except where non-compactness of a superdirective sound field was suspected. Directivity lines according to Equation (7) were added to Fig. 8. Their levels were adjusted to the levels of the directivities resulted from Powell's formulation, achieving excellent agreement in the form and less than 0·5dB difference in overall particularly for the circular jet. It is seen that the Powell's formulation managed to yield a profile more similar to that of Equation (7) than the Lighthill's formulation, thus pointing to the potential in Powell's formulation once the boundary correction issue is properly addressed.

3.2 Planar jet

Planer jets were simulated with the assumption of a simple nozzle of a duct form. This was done in order to capture the evolution of the jet inside the nozzle and to consider the effect of synthetic jets on the primary jet. These results will be reported somewhere else. The inflow profile was set either to a parabolic or a top-hat with a Pohlhausen correction to account for the effect of the nozzle walls. The inflow profile was perturbed in a similar way as in the circular and elliptic jet simulations but with 20 frequencies spaced between $0{\cdot}1 < \mathrm{St}_h < 0{\cdot}5$ where h is the width of the nozzle. The computational domain size and a typical breakdown of the flow structures are illustrated in Fig. 9. A typical LES grid size of $\Delta x = 0{\cdot}117h$, $\Delta y = 0{\cdot}62h$, $\Delta z = 0{\cdot}125h$ was used which was found to be slightly finer than previous compressible LES studies. Taking $L_z = 8h$ for the spanwise length of the computational domain was found to be sufficient to contain the large scale structures and to reduce considerably the dependency of the presented results on the spanwise length.

It was found that the parabolic inflow profile led to a breakdown of the flow structures through a 'snaky' mode while the top-hat profile led to a puffing mode, agreeing with a previous experimental study[21,30]. The downstream distribution of the time averaged centreline velocity $U_{c.l.}$ and the jet's half width b are plotted in Figs 10. Also plotted are the asymptotic linear lines for the self preserving region. These are:

$$b/h = K_1(x/h + K_2), \quad (U_0/U_{c.l})^2 = C_1(x/h + C_2) \quad \ldots (8)$$

Both jets of both inflow conditions have achieved this behaviour. The coefficients of these lines agree well with the range of published computational and experimental results. Further details on planar jet hydrodynamics are available in Supontisky *et al*[30].

The distributions of the RMS of the dominant longitudinal Q_{xx} Lighthill's quadrupoles are shown in Figs 11, where the RMS was averaged along the spanwise direction. Both cases of inflow profiles show a peak of the RMS after the potential cores as in the simulations of the circular and elliptic jets. The top-hat profile case shows a slightly earlier peak around $x = 6h$, although the end of the potential core was found to be almost the same as of the parabolic inflow profile.

The overall acoustic power spectrum is shown in Fig. 12. The results have been scaled to the conditions of Kouts and Yu's experiment[24] and have been normalised by the total acoustic power output and the spanwise length of the computational domain. A Doppler correction factor according to Lighthill's theory was added to our results in order to account for the finite Mach number of the experiment. There was no other adjustment in the results. Overall there is a good agreement between the prediction and the experimental result over the low frequency range. Unlike the parabolic inflow case which showed a distinctive peak[30] around St_h = 0·1 the shown spectra from the top-hat inflow profile do not, pointing to the effect of the inflow condition. The broad peak at low frequencies is wider than that seen in the frequency spectra of the circular and elliptic jets seen in Figs 6. At higher frequencies there is a much higher

https://doi.org/10.1017/S0001924000002360 Published online by Cambridge University Press

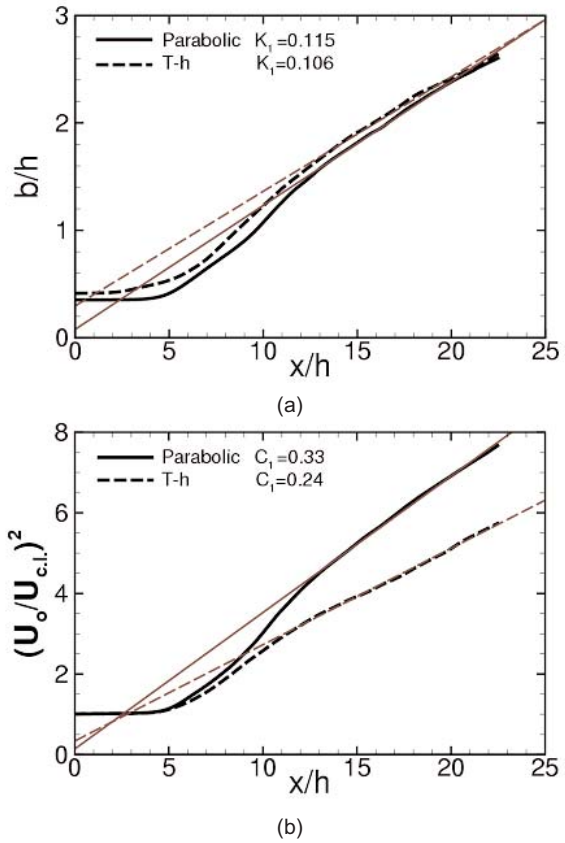


Figure 10. Streamwise evolution of the planar jet of Re_h = 3,000 for (a) mean centreline velocity and (b) jet's half width.

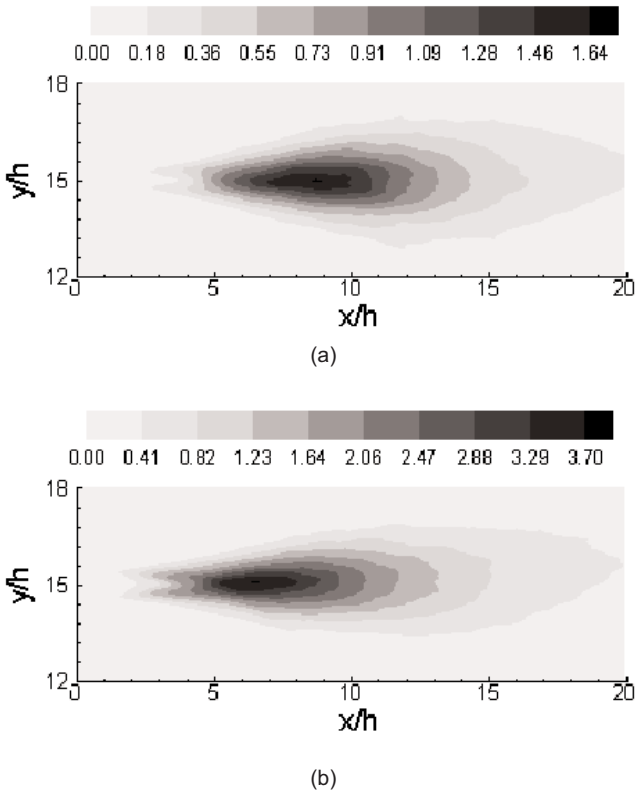


Figure 11. Contours of the RMS distribution of Lighthill's quadrupole Q_{xx} averaged in the spanwise direction for the planar jets of Figures 10 and (a) parabolic inflow profile and (b) top-hat inflow profile.

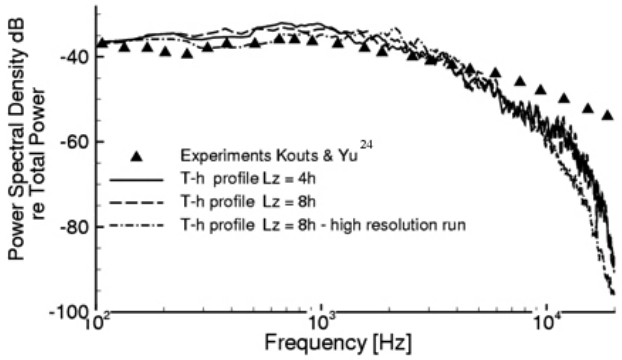


Figure 12. Acoustic power spectral density for the planar jet of Figure 10 and with a top-hat inflow profile.

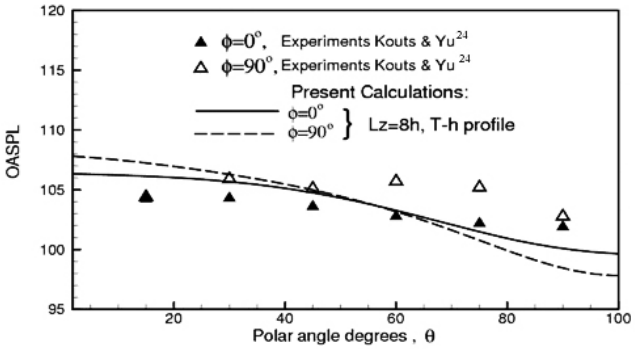


Figure 13. Directivities of the Over All Sound Pressure Level (OASPL) for the planar jet of Figure 12.

difference between the computed and experimental results for the planar jet. It is known that acoustic calculations based on LES data may have difficulties in predicting high frequency noise.

The overall directivity pattern is shown in Fig. 13 where ϕ is the spherical angle (ϕ = 90° points to the stream-normal direction). As in the circular and elliptical jets the highest sound emission is achieved in the streamwise direction. However the planar jet shows steeper decay in the directivity towards the stream-normal direction than the circular and elliptical jets. There is good to fair agreement between the predictions and the experimental results for the planar jet as seen in Fig. 13. The moderate decrease in the experimental directivity towards the shallow polar angles was not captured by our predictions. This may be due the omission of shear refraction in the current calculations. However the shown results show saturation in the level towards the shallow angle while previous results based on the parabolic inflow profile showed increase towards the shallow angles[30], pointing again to the effect of the inflow condition.

SUMMARY

Hydrodynamic and acoustic calculations were presented for low speed circular, elliptic and planar jets. The indirect approach was used, where the flow field was simulated using the incompressible LES approach. The emitted sound was calculated using two

https://doi.org/10.1017/S0001924000002360 Published online by Cambridge University Press

formulations of Lighthill's acoustic analogy: The velocity stress tensor formulation of Lighthill and the vortex sound formulation of Powell. Consideration was given to the fact that the computational domain was finite. A new boundary correction for Powell's formulation was developed to account for it.

Results were presented for various Reynolds numbers ranging from low to moderate. All showed flow transition to turbulence and a breakdown of the large scale flow structures to smaller scales. Good qualitative and quantitative agreements with published results on the flow development were achieved. They pointed to higher mixing and axis switching in the elliptic jet and to the effect of the inflow profile on the breakdown mechanism of planar jets. Some statistics on the centreline velocity and the jets' spreading was also presented and compared with known results.

The new boundary correction for Powell's acoustic formulation was found to be essential in order to achieve good agreement with the prediction of Lighthill's formulation for the circular and elliptic jets. Without it a difference of up to 20dB between the two formulations was recorded. When using the new boundary correction the difference was reduced to less than 1dB. Both formulations managed to achieve the f^{-2} asymptotic drop for high frequencies. Both formulations also showed that the circular jet noise level is about 2dB higher than the elliptic jet and thus changing the nozzle geometry from circular to elliptic may not be a very effective method to achieve noise reduction at least for the conditions investigated in this study. Acoustic calculations for the planar jet managed to achieve fair to good agreement with published experimental results at least for low frequencies.

The current acoustic calculations were limited to basic sound patterns, meaning convection and shear refraction effects were neglected (although convection effects were added later for the planar jet results using Lighthill's Doppler correction). These effects can be included using for example Lilley's equation although care must be taken if this equation is simulated in time due to a lack of dissipation mechanism in the equation[17]. Of course higher Reynolds number simulations are needed and these will become easier as computational power increases. However, although some success was noticed in capturing relatively high frequency noise of circular and elliptic jets, a significant challenge remains and that is to improve the aeroacoustic predictions for high frequency when using LES results.

ACKNOWLEDGEMENTS

The authors are grateful for EPSRC for providing national computing time under grant EP/D044073/1. Dr. Suponitsky is grateful for the EC Marie Curie programme for supporting her work in Queen Mary, University of London under grant 0111415.

REFERENCES

1. LIGHTHILL, M.J. On sound generated aerodynamically: I. General theory. *Proc R Soc Lond,* 1952, **A211**, pp 564-587.
2. LILLEY, G.M. On the noise from air jets, 1958, ARC 20376, F.M. 2724.
3. POWELL, A. Theory of vortex sound, *J Acous Soc Am,* 1964, **36**, (1), pp 177-195.
4. MÖHRING, W. On vortex sound at low Mach number, *J Fluid Mech*, 1978, **85**, pp 685-691
5. LILLEY, G.M. On the noise from jets 1974. AGARD CP-131, pp 13-1 to 13-12.
6. LIGHTHILL, M.J. *The final panel discussion in Computational Aeroacoustics,* HARDIN, J.C. and HUSSAINI, M.Y. (Eds), Springer-Verlag, NY, USA, 1993.
7. WANG, M., FREUND, J.B. and LELE, S.K. Computational prediction of flow-generated sound, *Annual Review Fluid Mech*, 2006, **38**, pp 483-512.
8. CRIGHTON, D.G. *Computational Aeroacoustics for Low Mach Number Flows in Computational Aeroacoustics* HARDIN, J.C. and HUSSAINI, M.Y. (Eds), Springer-Verlag, NY, USA,1993.
9. SUPONITSKY, V., AVITAL, E.J. and GASTER, M. On three dimensionality and active control of incompressible cavity flow, 2005, *Phys Fluids*, **17**, (10), pp 104, 103.
10. LAI, H. and LUO, K.H. A three-dimensional hybrid LES-Acoustic analogy method for predicting open-cavity noise, *Flow Turbulence Combustion*, 2007, **79**, (1), pp 55-82.
11. CROW, S.C. and CHAMPAGNE, F.H. Orderly structure in jet turbulence. *J Fluid Mech*, 1971, **48**, (3), pp 547-591.
12. KIBENS, V. Discrete noise spectrum generated by an acoustically excited jet, *AIAA J,* 1980, **18**, (4), pp 431-441.
13. LAUFER, J. and YEN, T.C. Noise generation by a low Mach number jet. *J Fluid Mech*, 1983, **134**, pp 1-31.
14. CRIGHTON, D.G. and HUERRE, P. Shear-layer pressure fluctuations and superdirective acoustic sources, *J Fluid Mech*, 1990, **220**, pp 355-368.
15. AVITAL, E.J. and SANDHAM, N.D. Note on the structure of the acoustic field emitted by a wave packet, *J Sound Vib*, 1997, **204**, (3), pp 533-539.
16. AVITAL, E.J., SANDHAM, N.D., LUO, K.H. and MUSAFIR, R.E. Calculation of basic sound radiation of axisymmetric jets by direct numerical simulation. *AIAA J*, 1999, **37**, (2), pp 161-168.
17. JIANG, X., AVITAL, E.J. and LUO, K.H. Direct computation and aeroacoustic modelling of a subsonic axisymmetric jet, *J Sound Vib*, 2004, **270**, pp 525-538.
18. HO, C.M. and GUTMARK, E. Vortex induction and mass entrainment in a small-aspect-ratio elliptic jet, *J Fluid Mech*, 1987, **179**, pp 383-405.
19. BRIDGES, J.E and HUSSAIN, A.K.M.F. Roles of initial condition and vortex pairing in jet noise, *J Sound Vibr*, 1986, **117**, (2), pp 289-311.
20. TAM, C.K. and ZAMAN, K.B.M.Q. Subsonic jet noise from non-axisymmetric and tabbed nozzles, *AIAA J*, 2000, **38**, (4), pp 592-599.
21. SATO, H. The stability and transition of a two-dimensional jet, *J Fluid Mech*, 1960, **7**, pp 53-80.
22. MUMFORD, J.C. The structure of the large eddies in fully developed turbulent shear flows. Part 1: The plane jet, *J Fluid Mech*, 1982, **118**, pp 241-268.
23. STANELY, S.A, SARKAR, S. and MELLADO, A. Study of the flow-field evolution and mixing in a planar turbulent jet using direct numerical simulation, *J Fluid Mech*, 2002, **450**, pp 377-407.
24. KOUTS, C.A. and YU, J.C. Far noise field of a two-dimensional subsonic jet, *AIAA J*, 1975, **13**, pp 1031-1035.
25. MUNRO, S.E. and AHUJA, K.K. Aeroacoustics of a high aspect-ratio jet, 9th AIAA/CEAS Aeroacoustics conf., 2003, AIAA paper 2003-3323, South Carolina, USA.
26. ABRAMOWITZ, M. and STEGUN, I.A. *Handbook of Mathematical Functions*, Dover Publications, New York, USA, 1972
27. AVITAL, E.J. A second look at the role of the fast Fourier transform as an elliptic solver, *Int J Num Meth Fluids*, 2005, **48**, (9), pp 909-927.
28. KIM, W.W. and MENON, S. An unsteady incompressible Navier-Stokes solver for large eddy simulation of turbulent flow, *Int J Num Meth Fluids*, **31**, pp 963-1017.
29. INAGAKI, M., KONDOH, T. and NAGANO, Y. A mixed-time-scale SGS model for practical LES. *Trans Japan Soc Mech Eng,* 2002, Part B. **68**, (673), pp 2572-2579.
30. SUPONTISKY, V., AVITAL, E. and GASTER, M. Hydrodynamics and sound generation of low speed planar jet, *J Fluid Eng* (in press).
31. MICHALKE, A. Survey on jet instability theory. *Prog Aerospace Sci,* 1984, **21**, pp 159-199.
32. LILLEY, G.M. The radiated noise from isotropic turbulence with applications to the theory of jet noise. *J Sound Vib*, 1996, **190**, (3), pp 463-476.
33. MUSAFIR, R.E. On the sound field of organized vorticity in jet flows, 13th Int. Congress on Acoustics, 1989, **2**, pp 63-66.

APPENDIX A – BOUNDARY CORRECTIONS FOR POWELL'S FORMULATION.

Let us take the Powell's source as

$$\ddot{\theta}_{1j} = \frac{\partial^2}{\partial t^2}\int (y_1 - y_{01})(\bar{\omega}\times\bar{u})_j \,d\bar{y} + \int_{S_{out}} (y_1 - y_{01}) f_j \,ds - \int_{S_{in}} (y_1 - y_{01}) f_j \,ds \quad \ldots (A1)$$

where S_{out} is the outlet surface area of the computational domain and Sin is the inlet. The last two terms of the right hand side of Equation (A1) are the boundary corrections. Their forms are similar to those using for the Möhring's vortex sound formulation by Avital *et al*[16] for the axisymmetric case. In order for Equation (A1) to be

https://doi.org/10.1017/S0001924000002360 Published online by Cambridge University Press

independent of the location of the co-ordinate origin in the streamwise direction y_{01}, one needs to have;

$$\frac{\partial^2}{\partial t^2}\int(\bar{\omega}\times\bar{u})_j\,\mathrm{d}\bar{y}+\int_{S_{out}}f_j\,\mathrm{d}s-\int_{S_{in}}f_j\,\mathrm{d}s \qquad \ldots\ (A2)$$

Introducing the vector identity;

$$\nabla\left(\frac{|u|^2}{2}\right)-(\bar{u}\times\bar{\omega})=(\bar{u}\cdot\nabla)\bar{u} \qquad \ldots\ (A3)$$

and so for $j = 1$ one gets,

$$(\bar{\omega}\times\bar{u})_1=\frac{1}{2}\frac{\partial}{\partial x_1}\left(u_1^2-u_2^2-u_3^2\right)+\frac{\partial(u_1u_2)}{\partial x_2}+\frac{\partial(u_1u_3)}{\partial x_3} \qquad \ldots\ (A4)$$

Introducing Equation (A4) into Equation (A2) and assuming that in the stream-normal x_2 and spanwise x_3 directions the computational domain is large enough so the flow decays sufficiently to make u_1u_3 and u_1u_3 close to zero, one gets

$$\frac{\partial^2}{\partial t^2}\int(\bar{\omega}\times\bar{v})_1\,\mathrm{d}\bar{y}\cong\frac{1}{2}\frac{\partial^2}{\partial t^2}\left[\int_{S_{out}}\left(u_1^2-u_2^2-u_3^2\right)\mathrm{d}s-\int_{S_{int}}\left(u_1^2-u_2^2-u_3^2\right)\mathrm{d}s\right] \qquad \ldots\ (A5)$$

Therefore,

$$f_1=-\frac{1}{2}\frac{\partial^2\left(u_1^2-u_2^2-u_3^2\right)}{\partial t^2} \qquad \ldots\ (A6)$$

Similarly, for $j = 2$ one gets from Equation (A4) that

$$(\bar{\omega}\times\bar{u})_2=\frac{1}{2}\frac{\partial}{\partial x_2}\left(u_2^2-u_1^2-u_3^2\right)+\frac{\partial(u_2u_1)}{\partial x_1}+\frac{\partial(u_3u_1)}{\partial x_3} \qquad \ldots\ (A7)$$

Similar analysis leads to

$$f_2=-\frac{\partial^2(u_1u_2)}{\partial t^2} \qquad \ldots\ (A8)$$

and consequently,

$$f_3=-\frac{\partial^2(u_1u_3)}{\partial t^2} \qquad \ldots\ (A9)$$

https://doi.org/10.1017/S0001924000002360 Published online by Cambridge University Press